Available online at www.sciencedirect.com

SciVerse ScienceDirect

journal homepage: www.elsevier.com/locate/watres

An experimental study on the aggregation of TiO_2 nanoparticles under environmentally relevant conditions

Marina Belen Romanello [a,b,*], *Maria M. Fidalgo de Cortalezzi* [a,b]

[a] *Department of Chemical Engineering, Instituto Tecnológico de Buenos Aires, Av. Madero 399, Buenos Aires, Argentina*

[b] *CONICET, Argentina*

ARTICLE INFO

Article history:
Received 31 May 2012
Received in revised form
28 September 2012
Accepted 18 November 2012
Available online 22 March 2013

Keywords:
Nanoparticles
DLVO theory
Aggregation
Stability
Divalent cations
Natural organic matter

ABSTRACT

The eventual future scenario of a release of nanomaterials into the environment makes it necessary to assess the risk involved in their use by studying their behavior in natural waters. NanoTiO_2 is one of the most commonly employed nanomaterials. In the present work we studied the aggregation rates, aggregate size and aggregate morphology of NanoTiO_2 under the presence of inert electrolytes, divalent cations, and these two combined with natural organic matter, in an effort to provide a comprehensive investigation of the phenomena of interaction of nanomaterials and natural waters and elucidate some of the conflicting information reported in the literature. The stability of nanoparticles could be explained in all cases, at least qualitatively, in terms of classical DLVO interactions (Electrical Double Layer, Van der Waals). Divalent cations were adsorbed to the surface of the nanoparticles, neutralizing the negative charge at pH values greater than the point of zero charge and inducing aggregation. Natural organic matter (NOM) adsorbed to the particles and made their zeta potential more negative, hence stabilizing them by lowering the pH of maximum aggregation. Divalent cations partially neutralized the adsorbed NOM, and at high concentrations aggregation was observed with Ca^{2+} but not Mg^{2+}, suggesting the presence of specific Ca^{2+}–NOM bridges. SEM images visually revealed a fractal-like morphology of the aggregates formed under unfavorable conditions.

1. Introduction

With the continuing growth of nanotechnology and nanomaterials being applied more and more in consumer products, the scenario where these materials reach the natural environment is a highly likely one for the near future (Biswas and Wu, 2005). In order to accurately assess the risk involved in the use of nanotechnology and consider eventual environmental liabilities associated with it, a thorough understanding of the behavior of nanoparticles in natural waters is needed. Nanoparticles are expected to undergo different transformations under conditions commonly encountered in the environment (Klaine et al., 2008). As a consequence of their large area to volume ratio, surface dependent phenomena are very likely going to be dominant in determining their fate and transport in natural waters. Nanomaterials have very active surfaces, and therefore will have the tendency to adsorb molecules naturally present in waters, e.g. humic substances, but also may associate with pollutants and become transport facilitators for otherwise less mobile compounds. Another

* *Corresponding author*. Department of Chemical Engineering, Instituto Tecnológico de Buenos Aires, Av. Madero 399, Buenos Aires, Argentina. Tel.: +54 11 6393 4800.
E-mail address: mromanel@itba.edu.ar (M.B. Romanello).

0043-1354/$ – see front matter © 2013 Elsevier Ltd. All rights reserved.
http://dx.doi.org/10.1016/j.watres.2012.11.061

result of the surface modification is the change in the key properties that rule aggregation and deposition phenomena, such as zeta potential, interparticle minimum distance limited by adsorption layers, and the appearance of other forms of non-DLVO interaction energies.

TiO_2 nanoparticles are within the most common nanomaterials, finding applications in cosmetics, paints, catalyst, and many other fields. NanoTiO_2 is expected to continue to grow in the next decade (Robichaud et al., 2009), and may eventually substitute the bulk form. Under these scenario, a projected of 2.5 million metric tons of nanoparticles will be produced every year, and eventually released to the environment under its many forms (Robichaud et al., 2009).

Several reports on the physicochemical properties and aggregation studies of nanoparticles can be found in the recent literature (Domingos et al., 2009b; Domingos et al., 2010; Keller et al., 2010; French et al., 2009; Ottofuelling et al., 2011; Zhang et al., 2009; Dunphy Guzman et al., 2006; Petosa et al., 2010). Aggregation of metal oxides nanoparticles are controlled by pH and its effect on surface potential, with increasing aggregation near the point of zero charge of the material (Domingos et al., 2009b; Dunphy Guzman et al., 2006). However, nanoparticles in the environment are very unlikely going to be found bare, and adsorbed compounds, e.g. natural organic matter (NOM) will determine the final size. It has been proposed that NOM adsorption may provide a steric repulsion force that could prevent aggregation and even produce disaggregation of colloid aggregates, so that nanoparticle dispersion may occur to a larger extent than expected originally (Domingos et al., 2009b; Mosley et al., 2003).

Studies have shown partial, conflicting or non-easily comparable information, either because they use different models as NOM, different types of TiO_2 nanoparticles (which, in turn, affects their stability, zeta potential and size), ionic strength or NOM concentrations used are too different to be comparable, or variable measuring approach for particle stability (Domingos et al., 2009b; Dunphy Guzman et al., 2006; French et al., 2009; Thio et al., 2011; Zhang et al., 2009). Moreover, studies to elucidate the mechanisms governing aggregation dynamics, including aggregation rates, aggregate size, and morphology of these nanomaterials under the effect of NOM, different electrolytes, and these two combined is still unavailable.

The objective of this work is to provide a complete characterization of the aggregation dynamics of TiO_2 nanoparticles under environmentally relevant conditions, investigating size, kinetics and morphology of the aggregates. Two different organic molecules were used as NOM model compounds (a phenolic and a carboxylic organic acid) to investigate the effect of chemistry functionality of the adsorbed layers on the stabilization effect previously reported by other researchers. Both Ca and Mg salts were evaluated as divalent electrolytes, using Mg^{2+} as a control to evaluate specific Ca^{2+}–NOM interactions and to assess the influence of this ion that has seldom been studied.

Most previously published studies evaluate aggregation state at equilibrium (influence of surface potential on aggregation and transport of titania nanoparticles) (Domingos et al., 2009b; Dunphy Guzman et al., 2006; Ottofuelling et al., 2011). Even if some kinetic aggregation measurements were carried out (Thio et al., 2011), French et al., 2009) an exhaustive study of aggregation rates under different solution chemistries was not done prior to this work. Under all conditions studied, aggregation rates and pseudo-equilibrium states were considered.

2. Theory

The aggregation process is determined by the total interaction energy between particles as they approach each other (V_{TOTAL}), which is described by the traditional DLVO theory (Elimelech et al., 1998). According to this theory, the stability of colloidal particles in aqueous environments is determined by the sum of Van der Waals interactions (V_{VdW}) and electrical double layer interactions (V_{EDL}). Van der Waals interactions were calculated without retardation, according to Equation (1).

$$V_{VdW} = \frac{-A \cdot a}{12 \cdot h} \qquad \text{(Elimelech et al., 1998)} \tag{1}$$

Where a is the primary aggregate radius, h is the minimum distance between particles, and A is the Hamaker constant, 5.35×10^{-20}J (Ackler et al., 1996; Lennart, 1997). This equation is only valid for h much smaller than a.

V_{EDL} was calculated according to the linear superposition approximation, a useful compromise between constant-number and constant-charge assumptions, according to equation (2).

$$V_{EDL} = \frac{a \cdot n_\infty \cdot k \cdot T \cdot G^2}{K^2} exp(-K \cdot h) \qquad \text{(Elimelech et al., 1998)} \tag{2}$$

$$n_\infty = 1000 \times N_A \times c \tag{3}$$

$$G = \tan h\left(\frac{z \cdot e \cdot P}{4 \cdot k \cdot T}\right) \tag{4}$$

$$K = 2.32 \cdot 10^9 \cdot \left(\sum c_i \cdot z_i^2\right)^{1/2} \tag{5}$$

Where k is the Boltzmann constant, T is the temperature and h is much smaller than a. Bulk number concentration (n_∞) is calculated according to equation (3) where c is the ion molar concentration. The parameter G is calculated according to equation (4), where z is the charge of the ions, P is the experimental *zeta* potential and e is the electron charge. The inverse Debye length (K) is calculated as shown in equation (5), where c_i is the ion molar concentration and z_i is the charge of the ion.

Equation (2) is only valid with $K \times h$ is much bigger than 1, which was verified, and only for symmetric electrolytes. However this, it was also used for asymmetric electrolytes due to the lack of a better approach.

3. Methods and materials

3.1. *TiO_2 suspension preparation*

The Aeroxide P25 TiO_2 nanoparticles were provided by the manufacturer (Evonik Degussa Corporation, Parsippany, NJ).

P25 is a hydrophilic fumed TiO_2, a mixture of the rutile and anatase forms with an average primary particle size of 21 nm, as reported by the manufacturer.

Particle suspensions were prepared in different solvent chemistries; indifferent electrolytes (NaCl, Sigma–Aldrich, Germany) and divalent cations ($MgCl_2$, Sigma–Aldrich, Germany; and $CaCl_2$, Anedra, Argentina). Two model compounds were used for NOM: tannic acid (TA) (Carlo Erba reagents, Italy), and humic acid (HA)(Aldrich, Germany). Stock solutions of the different aqueous matrixes were prepared. The conditions assessed were: no electrolyte, NaCl; $CaCl_2$; $MgCl_2$; NaCl + 0.1 mg/L TA; $CaCl_2$ + 1 mg/LTA; $CaCl_2$ + 0.5 mg/LTA; $MgCl_2$ + 1 mg/L TA; $MgCl_2$ + 0.5 mg/L TA; NaCl + HA 1 mg/L (as total organic carbon); $CaCl_2$ + HA 1 mg/L (as total organic carbon) (Table 1).

Ionic strength was fixed at 0.9 mM for all cases except in one assay carried out with $CaCl_2$ 1.5 mM + HA 1 mg/L as (total organic carbon), and one assay carried out with 6 mM NaCl + HA 1 mg/L as (total organic carbon). For all solutions, ultrapure type I water (resistivity 18 MΩ) was used.

All containers were previously washed and rinsed carefully to prevent dust particle interference. For each aggregation measurement, fresh aliquots (100 ml) of the previously mentioned stock solutions were taken at a time and their pH was adjusted, using NaOH (Anedra, Argentina) or HCl (Anedra, Argentina) solutions previously filtered through 0.22 μm Millipore filters. Special care was taken to add as little acid or base as possible for pH adjustment, and in no case were both acid and base added (that is to say, if for instance the pH was lowered excessively with HCl, then a new solution was prepared instead of correcting the pH with NaOH). Special care was taken to minimize the addition of acid or base for pH adjustment. In no case were both acid and base added. The maximum ionic strength change due to pH correction was 0.01 mM, corresponding to a shift from pH 5.5 (pH of the stock solution) to pH 9.

Once the pH stabilized, 2.5 mg TiO_2 was added to the solution and gently stirred to assure a homogeneous suspension. Final pH was recorded and aliquots taken for size and zeta potential measurement. No buffer was added, as opposed to previous publications (Thio et al., 2011; French et al., 2009; Domingos et al., 2009b; Ottofuelling et al., 2011) avoiding the addition of extra species that could eventually interact with the nanoparticles and interfere with the determinations. It is important to note that no stock nanoparticle suspension was used as opposed to previously reported work (French et al., 2009; Domingos et al., 2009b, Thio et al., 2011; Zhang et al., 2009; Ottofuelling et al., 2011). This was done in order to avoid aggregation in the concentrated stock suspensions, that could affect the aggregation assays even if sonicated.

Table 1 – Suspension matrixes tested. Symbol × represents kinetic aggregation assays have been carried out, (*) represents SEM images have been obtained of those solutions at different pH conditions and symbol – represents that matrix has not been tested.

	Without NOM	With NOM	
		Tannic acid (1 ppm)	Humic acid (1 ppm as TOC)
No electrolyte	×	–	–
NaCl 0.9 mM	× (*)	× (*)	×
$CaCl_2$ 0.3 mM	× (*)	×	×
$MgCl_2$0.3 mM	×	×	× (pH = 5)
NaCl 6 mM, pH 5	–	–	×
$CaCl_2$ 1.5 mM, pH5	–	–	×
$MgCl_2$ 1.5 mM, pH5	–	–	×

3.2. *Particle characterization*

Kinetic size measurements were performed by Dynamic Light Scattering (DLS) using a Zetasizer Nano ZS, Malvern, UK. Immediately after the suspensions were prepared, samples for size measurement were taken in disposable polystyrene cuvettes. Measurements were taken every 102–103 s for each sample without removing the cell, for approximately 1 h and 10 min. After that period aggregation seemed to slow down, even if samples would have not been completely stabilized, according to what was previously reported (Domingos et al., 2009a).

Laser Doppler velocimetry was applied to characterize the electrophoretic mobility (EPM) of the TiO_2 NPs in the various electrolyte solutions using a Malvern Zetasizer Nano ZS. Measured EPMs were converted to *zeta*-potential using the Smoluchowski equation (Elimelech et al., 1998):

$$U = \varepsilon\zeta/\mu$$

Where U is the electrophoretic mobility, ε is the dielectric constant of the solution, μ is its viscosity, and ζ is the zeta potential.

Disposable folded capillary cells were employed. The samples were taken from the freshly prepared suspensions, but measured after 1 h and 10 min when negligible increase in aggregate size was observed and therefore aggregation equilibrium was assumed.

TiO_2 suspensions were freshly prepared, as explained previously. A drop was placed over a gold-coated glass support and immediately dried to minimize local concentration effects such as the meniscus effect, that would otherwise lead the reorganization of the aggregated particles (Domingos et al., 2009a). SEM images were taken with Zeiss Supra 40 microscope. Images were analyzed using ImageJ 1.45s, Wayne Rasband National Institutes of Health, USA.

4. Results and discussion

According to Rayleigh's approximation, the intensity of light scattered by a particle (or aggregate) is proportional to the sixth power of its diameter. This causes large particles to scatter far more light than small particles (Hiemenz, 1986). Therefore DLS Z-average or intensity values tend to overestimate particle size and to overweight larger aggregates (Domingos et al., 2009a). Given the high polydispersity of the samples, number measurements were considered more representative of the real size distribution, as they correct to certain extent this overestimation (Hanus and Ploehn, 1999).

The sizes measured at the beginning of each assay, as well as the size observed under conditions of high particle stability, indicate that P25 TiO_2 nanoparticles form primary aggregates of around 200 nm–300 nm in diameter, in accordance with the literature (Jiang et al., 2009; Mandzy et al., 2005; Thio et al., 2011). As in this study no stock solution was prepared, this primary aggregation would not be due to an enhanced collision frequency due to a local high concentration, as previously suggested (Thio et al., 2011). Attempts to break down the aggregates by ultrasonication in order to obtain the primary particles were unsuccessful. This is consistent with previous observations, which suggest that P25 TiO_2 forms strong aggregates in aqueous media (Mandzy et al., 2005).

The kinetic analysis carried out was similar to that employed by Stankus et al. (2010) with some variations: the mode number-weighed hydrodynamic particle diameter (diameter at the peak) of the size distribution determinations taken every 103 s was plotted as a function of time elapsed from the first measurement. The first set of measurements was fitted to a linear model (Fig. S1, Supplementary data). The number of data points included was such that the highest R^2 value was obtained, and the slope of the fitted curve was taken as an indirect measure of particle aggregation velocity (Fig. S1, Supplementary data). Final aggregate size was estimated as an average of the last 6 measurements taken.

Triplicate assays were carried out for the condition of 0.9 mM and pH 7 at which fast aggregation was expected. An average aggregation rate of 0.3851 ± 0.0328 was obtained. Additionally the results reported met in all cases the quality criteria established by the software that controls the instrument (Dispersion Technology Software Software, Zeta sizer Nano, Malvern UK).

Aggregation kinetics and final aggregate size were assessed at different solution pHs for all the conditions tested, as pH determines surface ionization for mineral oxides, and controls their surface charge in the absence of preferential adsorption of ions in solution (Morrison and Ross, 2002).

4.1. *Aggregation under the presence of an indifferent electrolyte*

As shown in Fig. 1A, aggregation was negligible at every pH assessed in the cases where no electrolytes were added to the solution. On the contrary, for the 0.9 mM NaCl suspensions aggregation was observed at pH values near pH seven, but at pHs far from the pzc, virtually no aggregation was observed. This is consistent with the critical coagulation concentration at pH 6 and similar TiO_2 concentration, previously informed as 0.8 mM NaCl (Boncagni et al., 2009). Results show that an ionic strength of 0.9 mM is high enough for particles to show significant aggregation around the pzc, but low enough for the electrical double layer not to be too compressed, a situation in which particles would aggregate at every pH value. This constant value of ionic strength was therefore chosen for the subsequent determinations as it allows favorable and unfavorable aggregation conditions to be distinguished.

For the 0.9 mM NaCl suspensions, both the rate of aggregation and final aggregate size are at their peak around pH 6 to 8 (Figs. 1B and 2B). This observation is consistent with the

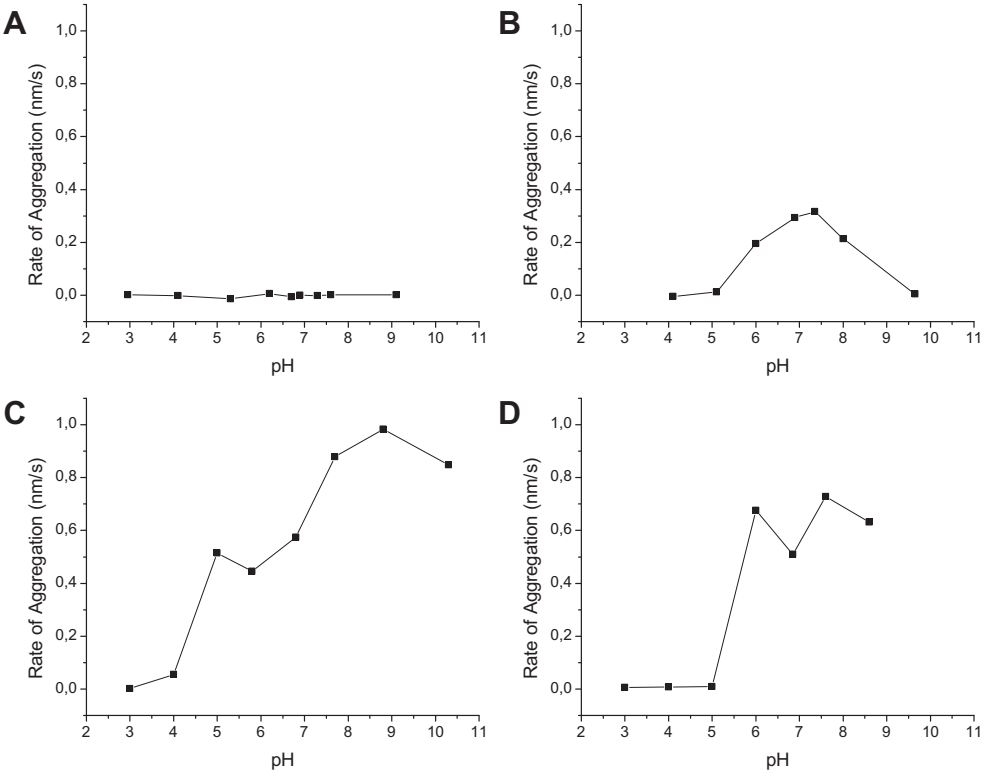

Fig. 1 – Aggregation rates as a function of pH in different solutions: (A) No electrolyte added (B) NaCl 0.9 Mm (pzc ≈ pH 6); (C) $CaCl_2$ 0.3 mM (pzc at pH ≥ 8); (D) $MgCl_2$ 0.3 mM (pzc at pH ≥ 8).

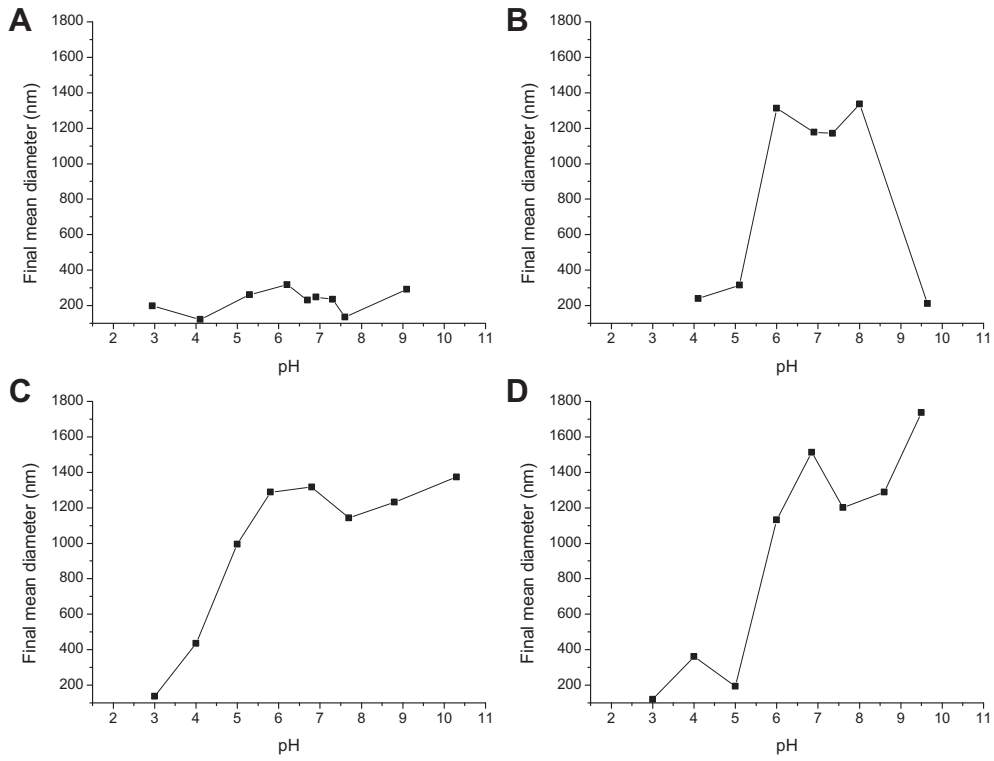

Fig. 2 – Final mean diameter, calculated as an average of the last 6 size measurements taken, as a function of pH, in different solutions: (A) No electrolyte added (B) NaCl 0.9 Mm (pzc around pH 6); (C) $CaCl_2$ 0.3 mM (pzc at pH ≥ 8); (D) $MgCl_2$ 0.3 m5M (pzc at pH ≥ 8).

point of zero charge (pzc) of the nanoparticles, which was found to be close to pH 6 (Fig. 3). Below this pH value, the oxygen atoms in the surface of TiO_2 nanoparticles would accept protons contributing to a positive zeta potential, and above this pH value hydrogen ions would be lost from the surface of the nanoparticles, contributing to a negative zeta potential (Stumm, 1992).

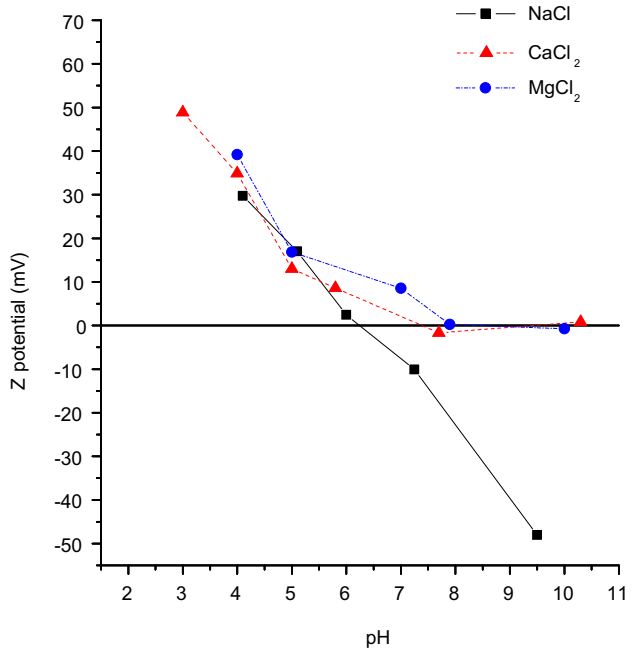

Fig. 3 – *zeta* potential as a function of pH in different solutions, with 0.9 mM ionic strength.

However, it can be noted from Fig. 1B that the maximum rate of aggregation for this condition was at pH 7, while the pzc was at pH 6. This last value coincides with previously reported values (Jiang et al., 2009; Kosmulski, 2002), suggesting that a slight shift in the pH may have occurred during measurements, as no buffer was used. Yet, in general terms, the results are in reasonable agreement with the predictions of the DLVO theory, calculated as explained in section 2. As shown in Fig. S2A of the supplementary data, attractive V_{TOTAL} is observed at pH 6 around the pzc, while repulsive interaction energies dominate at pH 9 where the particles are stabilized (Fig. S2B). The attractive V_{VdW} interactions are equal in both cases, since the primary aggregates are the same size, but the repulsive V_{EDL} energies vary as the particle *zeta* potential changes with pH. Fig. 1B shows that the closer the pH is to that corresponding to the pzc, the faster the rate of aggregation. This is explained by the DLVO theory since there is a significant decrease in the electrical double layer repulsive energy as the surface charge of the particles decreases. A similar trend is observed in the final size of the aggregates, and can be explained in the same way. However, Fig. 2A shows a subtle reduction in final size around pH 7, which is the pH of maximum observed rate of aggregation. This may be due to the formation of larger aggregates that may have settled out of suspension. Evolution of particle size with time for selected conditions tested is shown in Fig. S1 in the supplementary data.

4.2. *Aggregation under the presence of divalent cations*

Both in the case of presence of Ca^{2+} and Mg^{2+}, TiO_2 nanoparticles are stabilized at low pH values, and aggregate at high pHs at which they were stable in the NaCl solution, from pH 5 onwards for the case of Ca^{2+} (Figs. 1C and 2C), and from pH6 onwards for Mg^{2+} (Figs. 1D and 2D). The *zeta* potential stabilized close to a zero value at pHs above 7 (Fig. 3). This suggests that the divalent cations adsorb specifically to the surface of the nanoparticles, neutralizing the negative charges that would arise at basic pH and decreasing the absolute value of the *zeta* potential. This would account for the shift observed in the pzc under the presence of the divalent cations. The results can be explained under the light of the DLVO theory. At high pH values, the divalent cations neutralizing the negative surface charge lead to low electrical double layer repulsive interactions. Attractive Van der Waals interactions prevail, leading to net attractive force between particles, and thus particle aggregation. The interaction energies predicted by the DLVO theory for these cases are shown in the supplementary data, Fig. S3B. However, the observed rates of aggregation in these solutions were significantly larger than those observed for the NaCl solution. The Schulze–Hardy rule says that the CCC is inversely proportional to the square of the counterion charge for zeta potentials at which $ze\zeta/4\ kT < 1$ (which is the case for the nanoparticles in the suspensions studied) (Elimelech et al., 1998; Sposito, 2008). This means that the sodium to divalent cations CCC would be one fourth. Although this could account for the differences observed in the aggregation rates, the Na^{+} concentration assessed was three times that of Ca^{2+} and Mg^{2+}, which is not so different to the concentration the Schulze–Hardy rule states to be comparable. Therefore, although the increased aggregation rate under the presence of divalent cations could be explained by the higher compression of the double layer induced by divalent ions as opposed to monovalent ions, this does not rule out the possibility of specific interactions between the divalent cations and the nanoparticles.

The stability of the suspensions at low pH values can be explained by the DLVO theory: the divalent cations seem not to interact with the already positively charged surface of the nanoparticles and the *zeta* potential leads to electrostatic repulsion, reflected as a high electrical double layer interaction energy that overcomes the attractive Van der Waals forces (Fig. 3SA). Aggregation is therefore disfavored.

4.3. *Aggregation under the presence of natural organic matter and an indifferent electrolyte*

The effects of natural organic matter on the aggregation of TiO_2 nanoparticles were assessed using TA and HA as models of organic matter.

HAs are a heterogeneous group of polycarboxylic acids. As such, they have low pKa values, and through their carboxylate and phenolate groups they can form complexes with ions such as Mg^{2+} and Ca^{2+} (Ackler et al., 1996; Petosa et al., 2010). At natural water pHs, they are usually negatively charged. Due to its wide presence in the environment, HA are often employed as a model of NOM. TA is a polyphenol with a pKa value around 10. Moreover, given TA has no carboxyl groups, it is a good model for studying interactions with divalent cations between non-carboxylic acids in NOM.

Ionic strength was set at 0.9 mM with NaCl. Under the presence of TA the experimental pH of maximum aggregation shifted to pH 4 (Figs. 4A and 5A). This coincides with the new pzc established, given by a shift of the *zeta* potential curve toward lower pH values (Fig. 6). Given the high pKa of TA (around 10) and its low tendency of being protonated, we

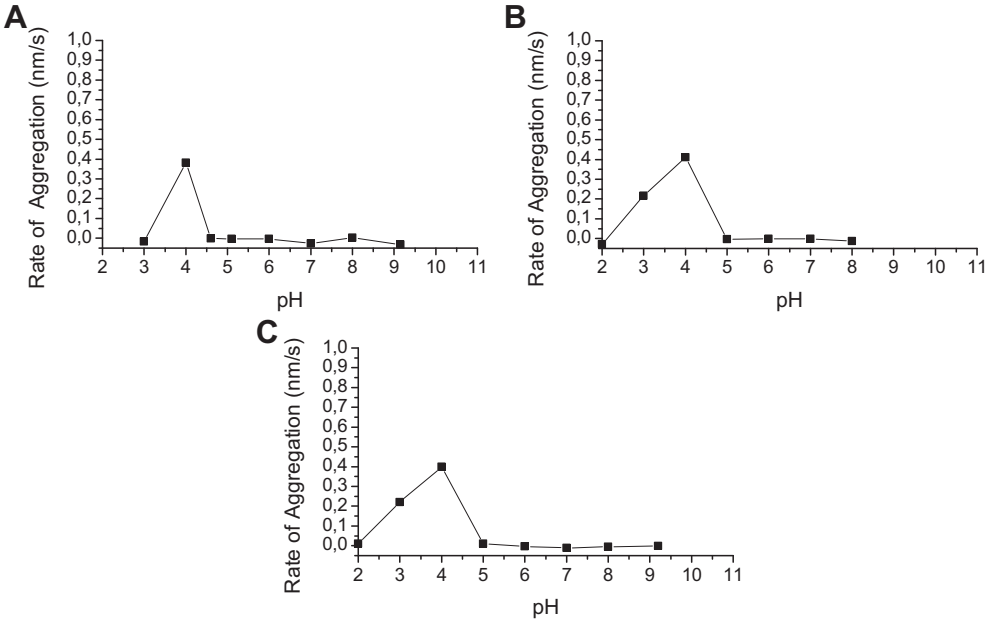

Fig. 4 – Aggregation rates as a function of pH in different solutions: (A) NaCl 0.9 mM + TA 1 mg/L (pzc ≈ pH 4); (B) $CaCl_2$ 0.3 mM + TA1mg/L (pzc ≈ pH 4); (C) $MgCl_2$ 0.3 mM + TA 1 mg/L (pzc ≈ pH 4).

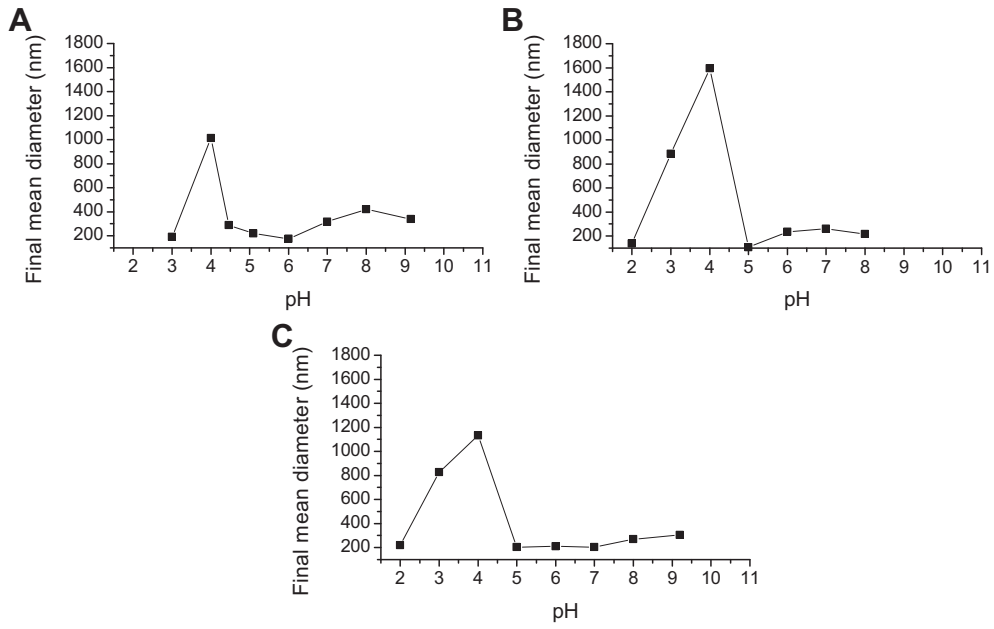

Fig. 5 – Final mean diameter, calculated as an average of the last 6 size measurements taken, as a function of pH, in different solutions: (A) NaCl 0.9 mM + TA 1 mg/L (pzc ≈ pH 4); (B) $CaCl_2$ 0.3 mM + TA 1 mg/L (pzc ≈ pH 4); (C) $MgCl_2$ 0.3 mM + TA 1 mg/L (pzc ≈ pH 4).

suggest that at the pH range tested TA is in its neutral form and the particle zeta potential is given solely by the proton exchange on the surface of the TiO_2 nanoparticles. The shift in the pzc would therefore correspond to an increased tendency of the nanoparticles to lose protons. We suggest that the hydroxyl groups in the TA might form hydrogen bonds on the surface of the nanoparticles reducing the tendency of the TiO_2 nanoparticles to accept protons. This should further be studied.

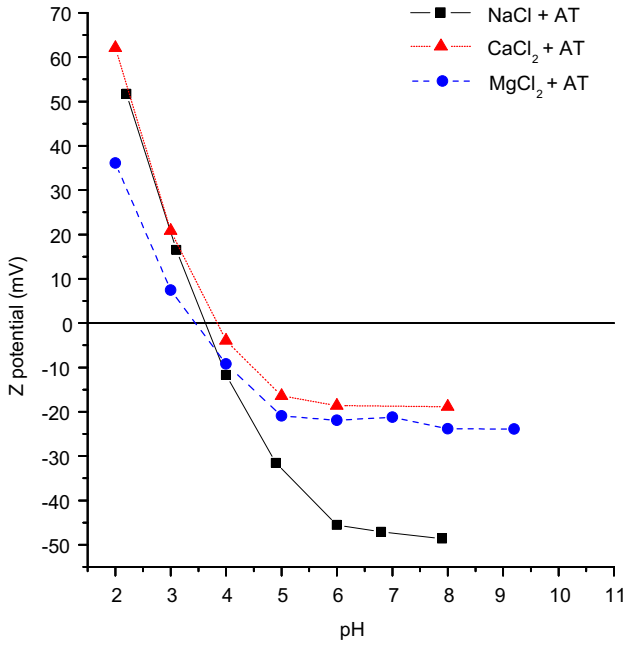

Fig. 6 – *zeta* potential as a function of pH in different solutions with 0.9 mM ionic strength and 1 mg/L TA.

As shown in Figs. 4A and 5A, nanoparticles were greatly stabilized at pH values other than 4, which is also in good agreement with the DLVO theory: at measured pH values other than 4, the *zeta* potential is far from the pzc, leading to a high repulsive electrical double layer interaction that stabilizes the particles.

In the case of HA, particles were stabilized at all of the pH values assessed (Figs. 7A and 8A). This coincides with the corresponding *zeta* potentials, which were all strongly negative (Fig. 9). It is suggested that HA in its anionic form adsorbs to the nanoparticle contributing to a total negative surface charge. This shift in Z potential was previously reported for TiO_2 as well as for other metal oxide nanoparticles (Mohammed, 2009; Ramos-Tejada et al., 2003). DLVO theory effectively explains these observations.

Natural organic matter therefore seems to have a general stabilizing effect upon TiO_2 nanoparticles, which coincides to previously reported results (Zhang et al., 2009; Chen et al., 2007; Mosley et al., 2003; Stankus et al., 2010; Thio et al., 2011).

4.4. *Aggregation under the presence of natural organic matter and divalent cations*

It has been previously reported that a specific intermolecular bridging between Ca^{2+} and NOM (Chen and Elimelech, 2008; Chen et al., 2007; Stankus et al., 2010) may enhance aggregation of nanoparticles in solutions containing these two species (Domingos et al., 2010). We therefore decided to test whether such cation could enhance aggregation of the TiO_2 nanoparticles in the presence of TA or HA. As Mg^{2+} was previously

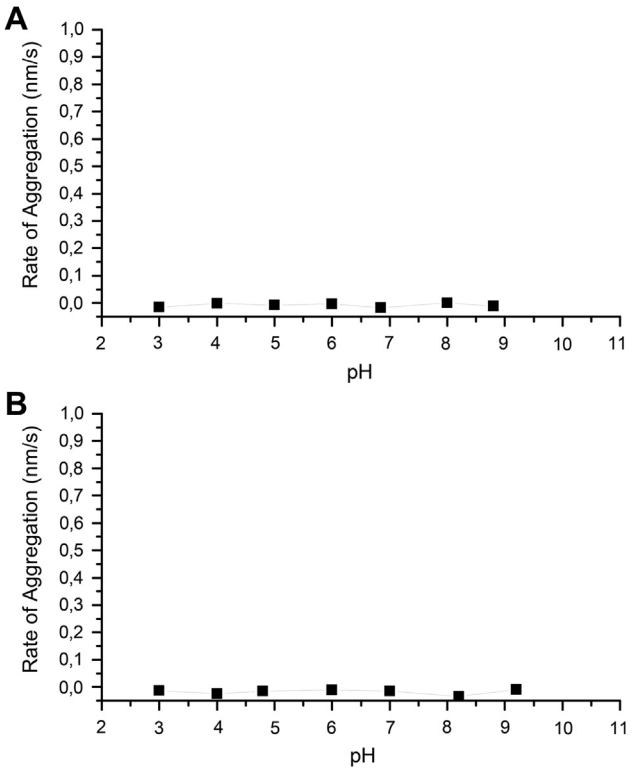

Fig. 7 – Aggregation rates as a function of pH in different solutions: (A) NaCl 0.9 mM + HA 1 mg/L as total organic carbon (pzc < pH 3); (B) $CaCl_2$ 0.3 mM + HA 1 mg/L as total organic carbon (pzc < pH 3).

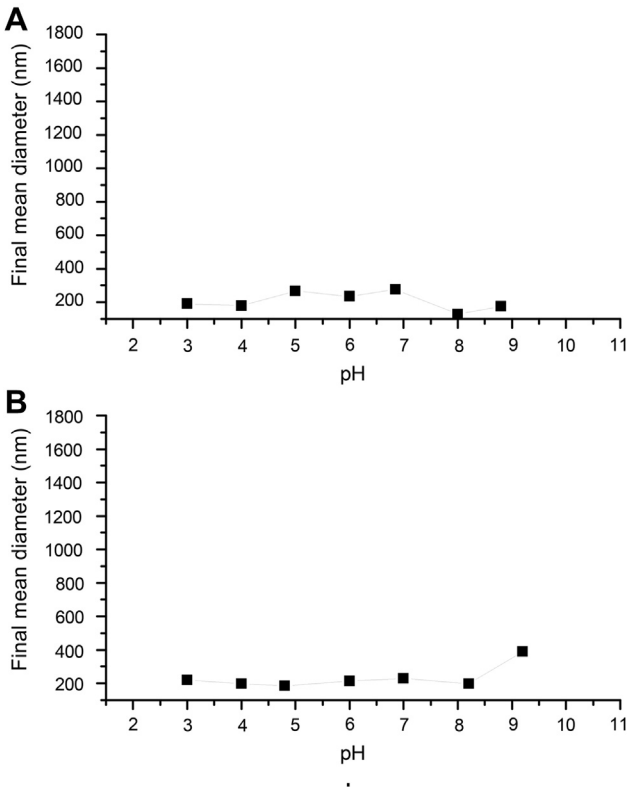

Fig. 8 – Final mean diameter, calculated as an average of the last 6 size measurements taken, as a function of pH, in different solutions: (A) NaCl 0.9 mM + HA 1 mg/L as total organic carbon (pzc < pH 3); (B) $CaCl_2$ 0.3 mM + HA 1 mg/L as total organic carbon (pzc < pH 3).

reported to interact with NOM differently or not at all (Chen and Elimelech, 2007; Stankus et al., 2010), it was used as a control. We therefore repeated the determinations using solutions of TA or HA and $CaCl_2$ or $MgCl_2$, keeping the ionic strength constant at 0.9 mM.

In the case of TA, the results showed no significant differences in nanoparticle aggregation in relation to what was observed with the indifferent electrolyte NaCl (Figs. 4A and B, 5A and B). However, the *zeta* potential curve did show some interaction between the TA and the divalent cations: the *zeta* potential remained fixed at about −20 mV for both cations, while it continued decreasing in the solution containing NaCl (Fig. 6).

In the case of HA, the results were similar: no difference was observed in the aggregation pattern in comparison to the case of NaCl (Figs. 7B and 8B), but the *zeta* potential was increased (Fig. 11). Similar results were previously reported (Thio et al., 2011). These results suggest that both kinds of divalent cations are interacting specifically with the NOM, neutralizing its negative charge at basic pH values, in a similar way to that described for the solutions with divalent cations and no NOM (Zhang et al., 2009). Finding this evidence of a specific NOM-divalent interaction, we hypothesized the bridging effect was not clearly observed due to an excess of free organic matter competing for the divalent cations and preventing the interaction with the molecules adsorbed to the nanoparticles. Moreover, it was previously reported that the

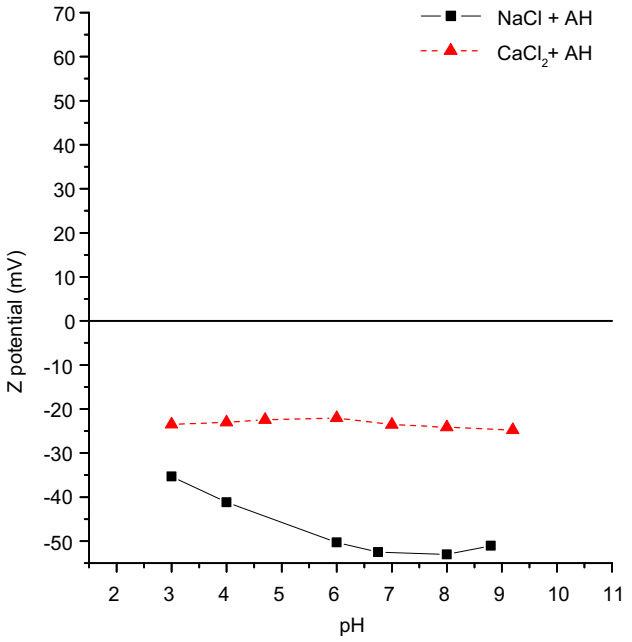

Fig. 9 – *zeta* potential as a function of pH in different solutions with 0.9 mM ionic strength and HA 1 mg/L as total organic carbon.

bridging between Ca^{2+} and NOM occurred at much higher cation concentrations (Chen and Elimelech, 2008; Chen et al., 2007; Stankus et al., 2010). However, even a mild increase in concentration would have a large effect in the ionic strength of the solution, producing a diminishing effect on the range of influence of the electrostatic repulsion forces and therefore inducing aggregation, regardless of any eventual specific interaction of the Ca^{2+} cation. We thus repeated the determination using half the amount of TA (0.5 mg/L), but no significant difference was observed. In addition, similar behavior was observed between Ca^{2+} and Mg^{2+}, as opposed to previously reported results (Chen and Elimelech, 2007). Yet, the fact that the presence of divalent cations increased the *zeta* potential would suggest that higher Ca^{2+} and Mg^{2+} concentrations could eventually neutralize the negative charge imparted by the NOM, leading to an additional mechanism for aggregation.

To test this hypothesis, we evaluated aggregation at a Ca^{2+} concentration of 1.5 mM and 1 mg/L HA as NOM, previously reported to be high enough to generate Ca^{2+} bridges (Ottofuelling et al., 2011), and repeated the assay replacing Ca^{2+} with Mg^{2+} as a control of specific calcium interactions. To account for the fact that divalent cations cause more compression in the double layer than monovalent cations as described by (Elimelech et al., 1998), we compared the aggregation under the presence of Ca^{2+} and Mg^{2+} with analogous aggregation assays where divalent cations were replaced with four times as much Na^{+} (6 mM). This relation coincides with the Schulze–Hardy rule. The pH in all cases was fixed at 5. The results showed aggregation occurred in the Ca^{2+} suspension (at a rate of 0.232 ± 0.014 based on two repetitions), but not in the Mg^{2+} or Na^{+} suspensions (Fig. S4, Supporting information). Aggregation was also assayed under 0.3 mM Mg^{2+} as a control, and it was found to be negligible as well. Moreover, the zeta potential measured in the Ca^{2+} suspension (−18.8 mV) did not show significant differences to that measured in the Mg^{2+} suspension (−19.4 mV). Furthermore, in neither of the three determinations did the zeta potential show significant differences with respect to the zeta potential previously measured at an ionic strength of 0.9 mM.

It has been previously suggested that the aggregation under the presence of Ca^{2+} but not Na^{+} could be due to the fact that, at these high ionic strength values, the electrical double layer is compressed and as the particle zeta potential is less negative in the suspension containing Ca^{2+} than in the one containing Na^{+}, the energy barrier for aggregation is lower in the first case (Ottofuelling et al., 2011; Zhang et al., 2009). However, if that was the case, aggregation should have also occurred under the presence of equivalent concentrations of Mg^{2+} as it is also a divalent cation and its size is similar to that of Ca^{2+}. Moreover, the fact that the zeta potential is similar both in the case of Ca^{2+} and Mg^{2+} implies that both cations neutralize to the same extent the negative charges in the HA. This would suggest, therefore, that the aggregation induced by Ca^{2+} ions would correspond to specific calcium–NOM interactions, and not to compression of the double layer thickness or reduction of NOM charge density as previously suggested (Ottofuelling et al., 2011; Thio et al., 2011), and that Mg^{2+} does not interact with HA in the same way.

It is important to highlight that the present work represents a very simplified model of environmental conditions. Therefore, even if at low pH values we found particles to be stabilized by positive zeta potentials, heterogeneous aggregation with, for instance, negatively charged clay colloids, could induce coagulation and thus remove the nanoparticles from suspension. The stability or settlement of the particles out of solution will therefore be highly dependent upon the complex matrix in which the particles are found. Further studies on this subject are recommended.

4.5. *Limitations of DLVO theory*

Although the DLVO theory proved to successfully explain the results, it is important to highlight the limitations in the application of this model. Particles are assumed to be hard spheres but they are actually non-spherical, porous aggregates that may have NOM or ions adsorbed to its surface. Moreover, for the V_{EDL} calculations, *zeta* potential was taken as the surface potential, for this latter cannot be experimentally determined. The sizes measured by DLS are in fact hydrodynamic diameters. The *zeta* potential was assumed to be determined for the surface of the hydrated particles for the V_{EDL} calculations; for the V_{VdW} calculations, the particle radius was approximated as the radius of hydration minus the adsorbed counterion diameter.

4.6. *Image analysis*

It is widely accepted that no single measuring technique can be employed for accurately determining nanoparticle sizes, specially for polydispersed samples (Domingos et al., 2009a). SEM images were taken as a tool for the validation of DLS particle size.

Images were taken for TiO_2 aggregates on the following conditions: NaCl 0.9 mM pH 4; NaCl 0.9 mM pH 6.7; $CaCl_2$ 0.3 mM pH 3; $CaCl_2$ 0.3 mM pH 10; NaCl 0.9 mM + TA 1 mg/L pH 6.8 (Table 1).

Image analysis revealed that the actual primary particle size seen by SEM is very similar to the particle size informed by the manufacturer, approximately 21 nm (Fig. 10).

In all cases, the sizes determined from the SEM images were similar to those measured by DLS, which can be taken as an indication of the good quality of the measurements as well as a correct preparation of the microscope samples.

Fig. 10 shows the primary aggregates formed in NaCl, $CaCl_2$ and NaCl + TA solutions, at pH values where aggregation is disfavored. The diameters of these aggregates coincide with the diameter measured by DLS, approximately 200 nm–300 nm. Fig. 11 shows aggregates formed in NaCl and $CaCl_2$ solutions at pH values where aggregation is favored. For these images, sizes ranged between 1000 nm and 3000 nm, also in good agreement with DLS data. However, some larger aggregates could also be distinguished that had not been detected by DLS. This is probably due to the fact that they fall outside the measuring range of the technique and/or settle out of suspension rapidly. Based on the images, the aggregates visually appear to be fractal: the primary aggregates from stable solutions shown in Fig. 10

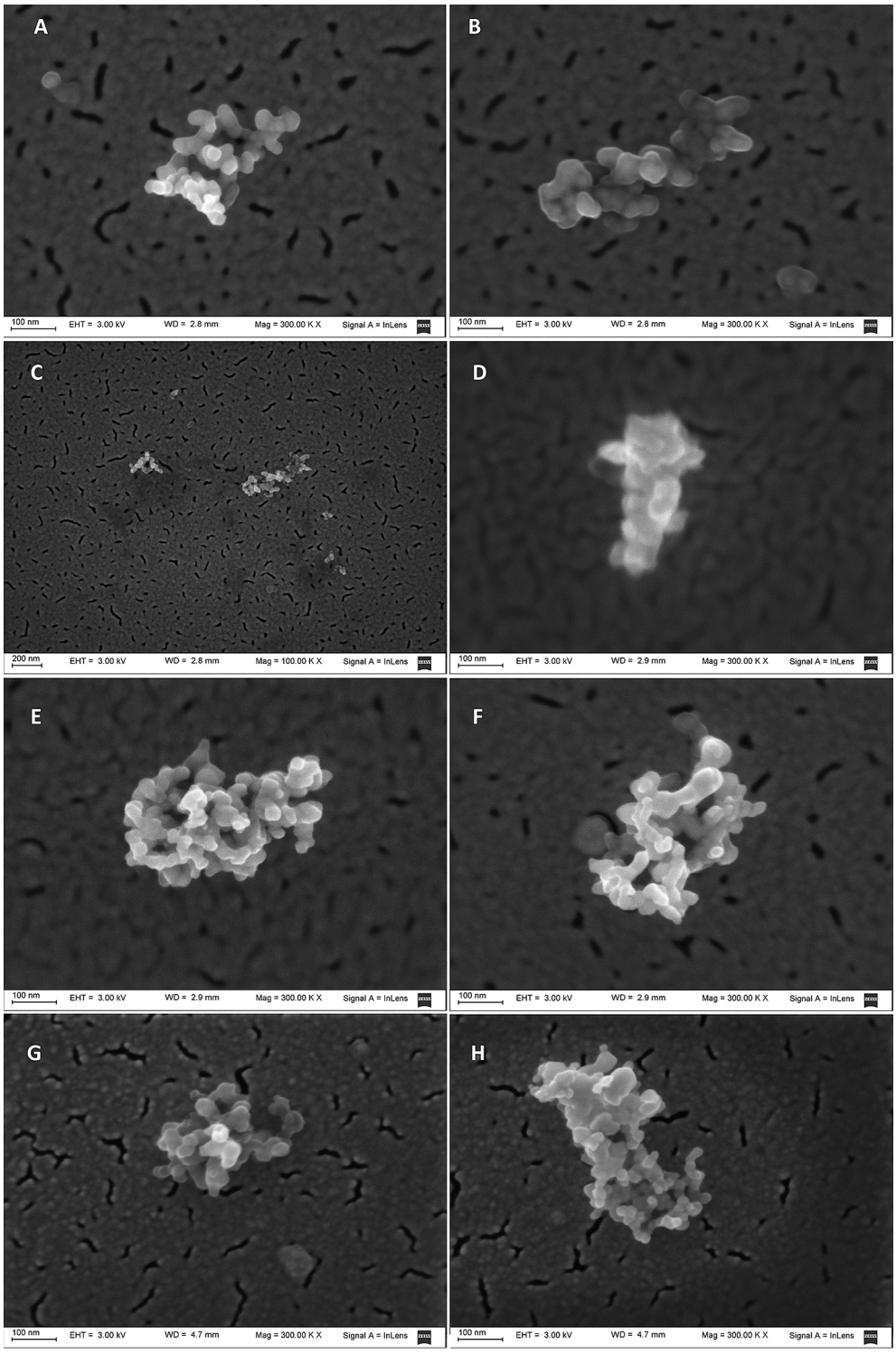

Fig. 10 – SEM images of TiO_2 primary aggregates prepared under stable solution conditions: (A) NaCl 0.9 mM, pH 4. 300,000×; (B) NaCl 0.9 mM pH 4. 300,000×; (C) NaCl 0.9 mM pH 4. 100,000×; (D) $CaCl_2$ 0.3 mM pH 3. 300,000×; (E) $CaCl_2$ 0.3 mM pH 3. 300,000×; (F) $CaCl_2$ 0.3 mM pH 9.2; (G) NaCl 0.9 mM + at 1 ppm pH 6.8. 300,000×; (H) NaCl 0.9 mM + at 1 ppm pH 6.8. 300,000×.

are relatively rounded and compact. This is a consequence of the high V_{EDL} repulsive interactions that result in a low sticking probability for collisions between particles. In contrast, the aggregates formed under unstable conditions (Fig. 11), showed an open, fractal-like morphology, with big pores, and even the substrate could be seen at a point through its structure. This can be explained by the attractive total interaction energy between particles under these

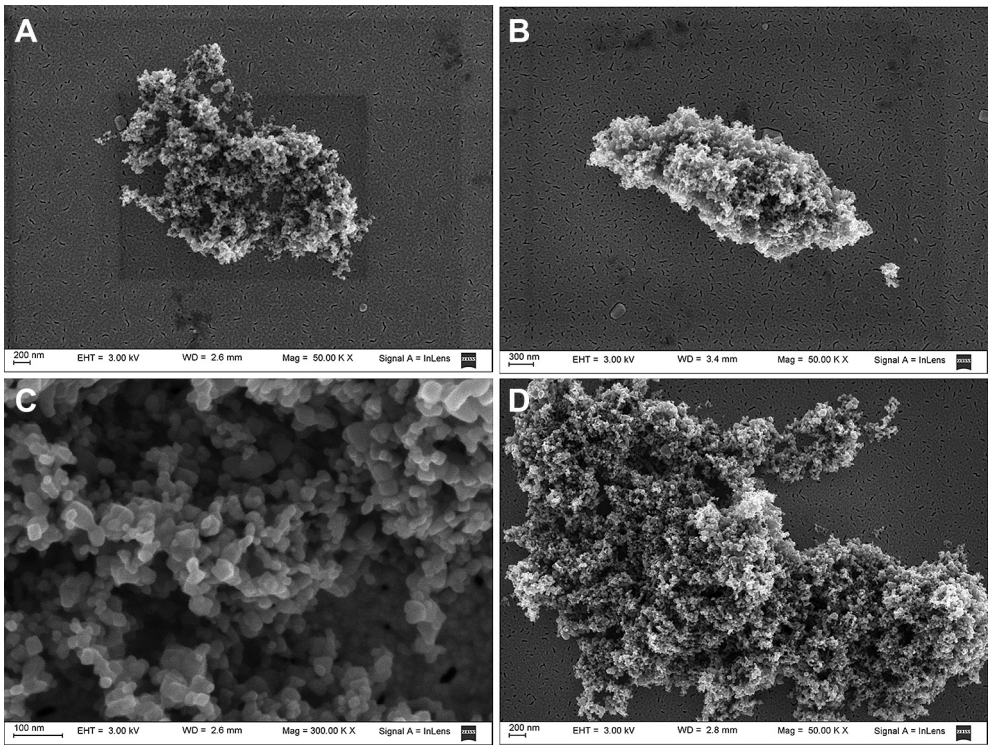

Fig. 11 – SEM images of TiO_2 final aggregates prepared under unstable solution conditions: (A) NaCl 0.9 mM, pH 6.7. 50,000×; (B) NaCl 0.9 mM pH 6.7. 50,000×; (C) NaCl 0.9 mM pH 6.7. 300,000×; (D) $CaCl_2$ 0.3 mM pH 3. 50,000×.

conditions, resulting in a high attachment efficiency (Elimelech et al., 1998).

5. Conclusions

- The characterizations of TiO_2 nanoparticles with respect to their size, rate of aggregation, surface charge, and aggregate morphology under a broad range of environmentally relevant conditions showed that these materials will undergo transformations after reaching natural waters and that the aqueous matrixes that they will encounter will largely determine their fate and transport in environment.
- The stabilization of nanoparticles could be explained in all cases, at least qualitatively, in terms of classical DLVO interactions (Electrical Double Layer, Van der Waals), with no consideration of any specific non-DLVO interactions, that although may be present in some cases, take a secondary role.
- In indifferent electrolyte solutions, TiO_2 nanoparticles form aggregates of approximately 200 nm–300 nm in size when under stable conditions (significant electrostatic repulsion forces present). However, they are rendered unstable and aggregate at and around neutral pHs due to the locations of pzc of the material.
- Divalent cations may cause aggregation at a wider range of pHs due to specific adsorption that prevents the surface charge to acquire negative values large enough to create a potential barrier to aggregation at pHs above the pzc, while their effect is negligible at pHs below the pzc.
- NOM has a stabilizing effect on the nanoparticles through adsorption of the mostly negatively charged compounds. However, under highly acidic conditions, they are expected to lose their stabilizing effect and particles may aggregate. The stabilization effect of NOM overrides the divalent ions influence toward aggregation at low cation concentrations (0.3 mM). However, at high cation concentrations (1.5 mM) enhanced aggregation is observed for Ca^{2+}, but not for Mg^{2+} suggesting the presence of specific Ca^{2+}–NOM interactions such as calcium bridges.
- SEM images of the aggregates validate the measurement data taken by DLS, and reflect some fractal behavior of the aggregation process. The observations can be explained through the attachment efficiencies of the particles and the DLVO interaction energies.

Acknowledgments

The authors acknowledge Center for Advanced Microscopy (CMA), Faculty of Natural and Exact Sciences, University of Buenos Aires for their help with the SEM images; ITBA, Agencia Nacional de Promoción Cientifica y Tecnológica under project PICT 2008-0566 and CONICET for partial funding; M. Romanello greatly acknowledges Banco Galicia for a graduate research fellowship.

Appendix A. Supplementary data

Supplementary data related to this article can be found at http://dx.doi.org/10.1016/j.watres.2012.11.061.

REFERENCES

Ackler, H.D., French, R.H., Chiang, Y.-M., 1996. Comparisons of Hamaker constants for ceramic systems with intervening vacuum or water: from force laws and physical properties. Journal of Colloid and Interface Science 179 (2), 460–469.

Biswas, P., Wu, C.Y., 2005. Nanoparticles and the environment. Journal of the Air & Waste Management Association 55 (6), 708–746.

Boncagni, N.T., Otaegui, J.M., Warner, E., Curran, T., Ren, J., Fidalgo de Cortalezzi, M.M., 2009. Exchange of TiO_2 nanoparticles between streams and streambeds. Environmental Science and Technology 43 (20), 7699–7705.

Chen, K.L., Elimelech, M., 2007. Influence of humic acid on the aggregation kinetics of fullerene (C60) nanoparticles in monovalent and divalent electrolyte solutions. Journal of Colloid and Interface Science 309 (1), 126–134.

Chen, K.L., Elimelech, M., 2008. Interaction of fullerene (C60) nanoparticles with humic acid and alginate coated silica surfaces: measurements, mechanisms, and environmental implications. Environmental Science and Technology 42 (20), 7607–7614.

Chen, K.L., Mylon, S.E., Elimelech, M., 2007. Enhanced aggregation of alginate-coated iron oxide (Hematite) nanoparticles in the presence of calcium, strontium, and barium cations. Langmuir 23 (11), 5920–5928.

Domingos, R.F., Baalousha, M.A., Ju-Nam, Y., Reid, M.M., Tufenkji, N., Lead, J.R., Leppard, G.G., Wilkinson, K.J., 2009a. Characterizing manufactured nanoparticles in the environment: multimethod determination of particle sizes. Environmental Science and Technology 43 (19), 7277–7284.

Domingos, R.F., Peyrot, C., Wilkinson, K.J., 2010. Aggregation of titanium dioxide nanoparticles: role of calcium and phosphate. Environmental Chemistry 7 (1), 61–66.

Domingos, R.F., Tufenkji, N., Wilkinson, K.J., 2009b. Aggregation of titanium dioxide nanoparticles: role of a fulvic acid. Environmental Science and Technology 43 (5), 1282–1286.

Dunphy Guzman, K.A., Finnegan, M.P., Banfield, J.F., 2006. Influence of surface potential on aggregation and transport of titania nanoparticles. Environmental Science and Technology 40 (24), 7688–7693.

Elimelech, M., Gregory, J., Jia, X., Williams, R., 1998. Particle Deposition and Aggregation: Measurement, Modelling and Simulation. Butterworth-Heinemann.

French, R.A., Jacobson, A.R., Kim, B., Isley, S.L., Penn, R.L., Baveye, P.C., 2009. Influence of ionic strength, pH, and cation valence on aggregation kinetics of titanium dioxide nanoparticles. Environmental Science and Technology 43 (5), 1354–1359.

Hanus, H.L., Ploehn, J.H., 1999. Conversion of Intensity-averaged Photon Correlation Spectroscopy Measurements to Number-averaged Particle Size Distributions. 1. Theoretical Development. American Chemical Society, Washington, DC, ETATS-UNIS.

Hiemenz, P.C., 1986. Principles of Colloid and Surface Chemistry. M. Dekker.

Jiang, J., Oberdörster, G., Biswas, P., 2009. Characterization of size, surface charge, and agglomeration state of nanoparticle dispersions for toxicological studies. Journal of Nanoparticle Research 11 (1), 77–89.

Keller, A.A., Wang, H., Zhou, D., Lenihan, H.S., Cherr, G., Cardinale, B.J., Miller, R., Ji, Z., 2010. Stability and aggregation of metal oxide nanoparticles in natural aqueous matrices. Environmental Science and Technology 44 (6), 1962–1967.

Klaine, S.J., Alvarez, P.J., Batley, G.E., Fernandes, T.F., Handy, R.D., Lyon, D.Y., Mahendra, S., McLaughlin, M.J., Lead, J.R., 2008. Nanomaterials in the environment: behavior, fate, bioavailability, and effects. Environmental Toxicology and Chemistry 27 (9), 1825–1851.

Kosmulski, M., 2002. The significance of the difference in the point of zero charge between rutile and anatase. Advances in Colloid and Interface Science 99 (3), 255–264.

Lennart, B., 1997. Hamaker constants of inorganic materials. Advances in Colloid and Interface Science 70 (0), 125–169.

Mandzy, N., Grulke, E., Druffel, T., 2005. Breakage of TiO_2 agglomerates in electrostatically stabilized aqueous dispersions. Powder Technology 160 (2), 121–126.

Mohammed, B., 2009. Aggregation and disaggregation of iron oxide nanoparticles: influence of particle concentration, pH and natural organic matter. Science of The Total Environment 407 (6), 2093–2101.

Morrison, I.D., Ross, S., 2002. Colloidal Dispersions: Suspensions, Emulsions, and Foams. Wiley-Interscience.

Mosley, L.M., Hunter, K.A., Ducker, W.A., 2003. Forces between colloid particles in natural waters. Environmental Science and Technology 37 (15), 3303–3308.

Ottofuelling, S., Von Der Kammer, F., Hofmann, T., 2011. Commercial titanium dioxide nanoparticles in both natural and synthetic water: comprehensive multidimensional testing and prediction of aggregation behavior. Environmental Science and Technology 45 (23), 10045–10052.

Petosa, A.R., Jaisi, D.P., Quevedo, I.R., Elimelech, M., Tufenkji, N., 2010. Aggregation and deposition of engineered nanomaterials in aquatic environments: role of physicochemical interactions. Environmental Science and Technology 44 (17), 6532–6549.

Ramos-Tejada, M.M., Ontiveros, A., Viota, J.L., Durán, J.D.G., 2003. Interfacial and rheological properties of humic acid/hematite suspensions. Journal of Colloid and Interface Science 268 (1), 85–95.

Robichaud, C.O., Uyar, A.E., Darby, M.R., Zucker, L.G., Wiesner, M.R., 2009a. Estimates of upper bounds and trends in nano-TiO_2 production as a basis for exposure assessment. Environmental Science and Technology 43 (12), 4227–4233.

Sposito, G., 2008. The Chemistry of Soils. Oxford University Press, USA.

Stankus, D.P., Lohse, S.E., Hutchison, J.E., Nason, J.A., 2010. Interactions between natural organic matter and gold nanoparticles stabilized with different organic capping agents. Environmental Science and Technology 45 (8), 3238–3244.

Stumm, W., 1992. Chemistry of the Solid–Water Interface: Processes at the Mineral–Water and Particle–Water Interface in Natural Systems. Wiley.

Thio, B.J.R., Zhou, D., Keller, A.A., 2011. Influence of natural organic matter on the aggregation and deposition of titanium dioxide nanoparticles. Journal of Hazardous Materials 189 (1–2), 556.

Zhang, Y., Chen, Y., Westerhoff, P., Crittenden, J., 2009. Impact of natural organic matter and divalent cations on the stability of aqueous nanoparticles. Water Research 43 (17), 4249–4257.